

SECTION 8

SUMMARY OF DAMPING IN AEROSPACE MATERIALS AND STRUCTURES

The typical damping levels in aerospace materials and the more common structures are summarized in this section. The levels quoted are not to be treated as absolute values, but more as an indication of the expected average damping values. In reality, there is considerable scatter in the measured damping data, especially for built up structures. A deviation from the quoted damping value of a factor of two, either way, is quite possible for these structures. A more detailed discussion on the nature of damping and the damping levels in the materials and some more common aerospace structures is contained in Section 7, Volume I of the design guide. A large list of references is also provided in that section for further study. This list also includes references for material damping in nonmetallic materials. Methods for measuring material damping are also discussed in some detail in that section since the damping values are generally very low and can be easily contaminated by the test method or the test apparatus.

All of the damping data in this section are presented in terms of the viscous damping ratio, ζ . The relationships between the more common damping expressions used in representing material damping are the loss factor (or structural damping), η , the logarithmic decrement, δ , the specific damping capacity, ψ , and the amplification factor, Q . These are related by

$$\eta = \frac{\psi}{2\pi} = \frac{\delta}{\pi} = \frac{1}{Q} = 2\zeta.$$

The damping data for aerospace metals are presented first followed by composites, metal matrix composites and aerospace structures. Much of the damping in stiffened panel type structures has been measured only for the fundamental mode. A method is provided by which the damping in the higher order modes can be estimated from the frequency and damping of the fundamental

mode. The commonly used one-over-the-frequency type variation of the damping with frequency is valid only if higher modes are included in such data. The damping in the fundamental mode of stiffened panel type structures is essentially constant with frequency. This behaviour has only recently been discovered [8.1] and verified by careful experiment [8.2].

Acoustic radiation damping also plays a greater role in the damping of riveted aluminum panels than originally thought. It is the dominant source of damping in stiffened aluminum and composite honeycomb panels [3.5]. Acoustic radiation is the only source of damping in integrally stiffened graphite/epoxy panels [8.3, 8.4] on account of the very low damping in graphite/epoxy material. The damping in these panels can now be predicted by theory [8.1, 8.5]. These developments are discussed in more detail both in Section 8.2 and in Section 7, Volume I of the design guide.

8.1 MATERIAL DAMPING IN AEROSPACE METALS AND COMPOSITES

8.1.1 Material Damping in Metals

The typical damping levels in the more common metals are listed in Table 8.1. In some of the metals, the material damping varies with dynamic stress amplitude [8.6, 8.7] as illustrated in [8.7] Figures 8.1 and 8.2. In some metals such as aluminum, the damping remains constant with stress level but is dependent on frequency, with maximum damping occurring at the relaxation frequency (see Section 7, Volume I). Some metals have especially high material damping values. These materials [8.8] are indicated in Figure 8.3 as a function of their Young's modulus for quick reference. Typical material damping values for steel and aluminum are included for comparison.

8.1.2 Material Damping in Composites with Epoxy or Polyester Matrix

The material damping in graphite, boron, Kevlar and glass fiber reinforced composites in, primarily, an epoxy matrix are presented in this section. The material damping is the lowest in unidirectional composite layups, with the fibers running parallel to the axial direction. Typical damping values are

listed in Table 8.2. The boron and graphite epoxy composites have the lowest material damping and Kevlar has the highest.

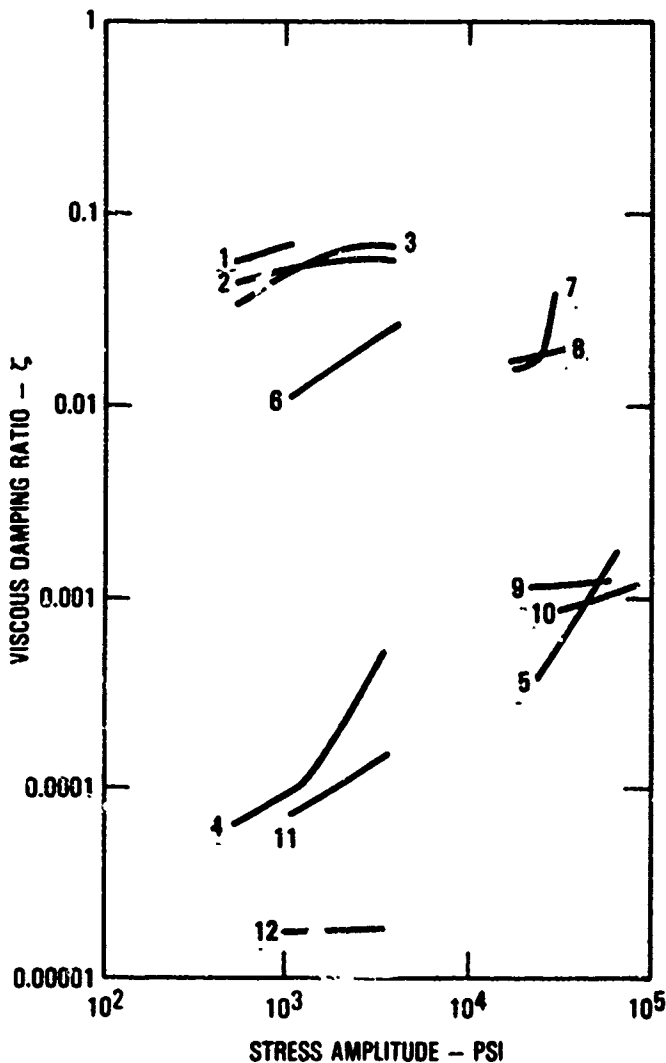
TABLE 8.1. TYPICAL MATERIAL DAMPING LEVELS IN METALS

MATERIAL	VISCOUS DAMPING RATIO ζ
Mild steel	0.0025 - 0.005
Alloy steel	0.0005 - 0.004
Aluminum alloy	0.00005 - 0.0012
Titanium alloy	≈ 0.0009

The damping in composites varies both with fiber volume as illustrated [8.9] in Figure 8.4 and with fiber orientation as illustrated in Figures 8.5 and 8.6 for graphite/epoxy [8.10] and Kevlar [8.2, 8.5], respectively. The material damping in composites, including the uniaxial composites, is derived entirely from the material damping in the matrix, as indicated in Table 8.3, in this instance for uniaxial aligned chopped fiber composites [8.11]. The damping in the uniaxial composites is not affected significantly by temperature [8.10]. For other fiber orientations, it follows the damping behaviour of the epoxy with temperature [Figure 8.7]. The shear (torsion) damping in composites is also high because of its dependence on the resin damping. The damping in axially aligned chopped fiber composites [8.11, 8.12, 8.13] can be increased by the use of progressively smaller fibers at the expense of a progressively reduced modulus. The variation of the damping in the composites with fiber orientation is predictable by theory [8.14, 8.15] based on the measured axial, transverse and shear damping values and the corresponding Young's moduli of uniaxial composites.

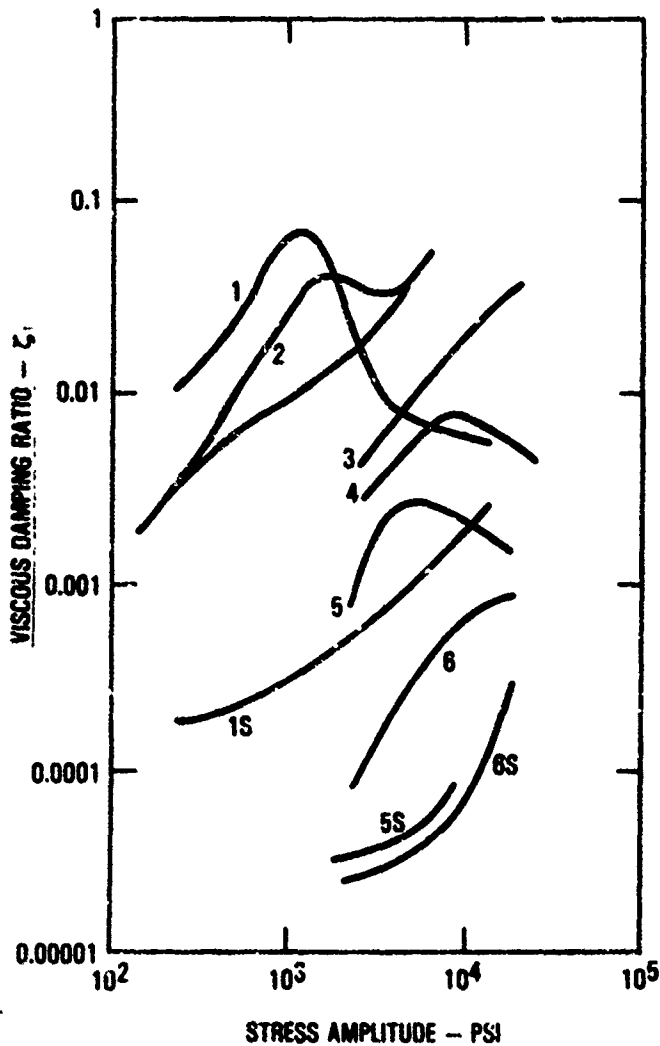
8.1.3 Metal Matrix Composites

The measured material damping in metal matrix composites is summarized in Table 8.4. A number of types of reinforcing fibers are used in, basically, an aluminum or magnesium matrix. The damping appears to be reasonably constant with frequency but does vary with both stress amplitude and temperature [8.16].



No.	MATERIAL
1	CAST MAGNESIUM 99.9% PURE
2	Mg - 0.6% Zn
3	Mg - 0.8%
4	Mg - 8.1% Al, 0.5% Zn, 0.2% Mn
5	AUSTENITIC STEEL OIL QUENCHED FROM 1000°C, 16 HOURS, 860°C
6	Mn - 35.9% Cu, 0.24% Fe, HEAT 1 HR, 790°C, QUENCH 2 HR, 450°C
7	N - 155 ALLOY, Fe 21.7% Cr, 1.9% W, 0.15% C, 19.4% Ni, 1.74% Mn, 19% Co, 0.78% Co, 2.75% Mo, 0.37% Si QUENCHED, AGED
8	STELLITE CO - 0.48% C, 1.4% Fe, 0.42% Mn, 24.8% Cr, 0.93% Si, 10.4% Ni, 7.28% W AS CAST
9	Ti - 3.9% Al, 4.3% Mn, 0.1% C ANNEALED
10	SANDVIK STEEL Fe - 1% Cr, 0.2% Si, 1% C, 0.28% Mn, 0.24% Mo, QUENCHED TEMPERED
11	Al - 5.5% Cu, 0.5% Fe, 0.5% Bi
12	Al - 4% Cu, 0.5% Mg, 0.5% Mn

Figure 8.1. Variation of the material damping in metals with dynamic stress amplitude.



No.	MATERIAL
1	Fe - 3.3% Si, ANNEAL 5.5 HR AT 1200°C
1S	SAMPLE 1 SATURATION MAGNETIC FIELD
2	PURE NICKEL
2S	SAMPLE 2 SATURATION MAGNETIC FIELD
3	INVC0 73.5% Co, 22.5% Ni, 1.8% Ti, 1.1% Zr
4	403 STEEL ALLOY Fe - 12% Cr, 5% Ni
5	MILD STEEL 0.28% C, 0.2% Si, 0.76% Mn, 0.12% Cu, 0.14% Ni, 0.1% Cr, ANNEALED 18 HRS AT 625°C
5S	SAMPLE 5 SATURATION MAGNETIC FIELD
6	CARBON STEEL 0.42% C, 0.32% Si, 0.99% Mn, 0.09% Ni, 0.06% Cr, NORMALIZED
6S	SAMPLE 6 SATURATION MAGNETIC FIELD

Figure 8.2. Variation of the material damping with dynamic stress amplitude in metals.

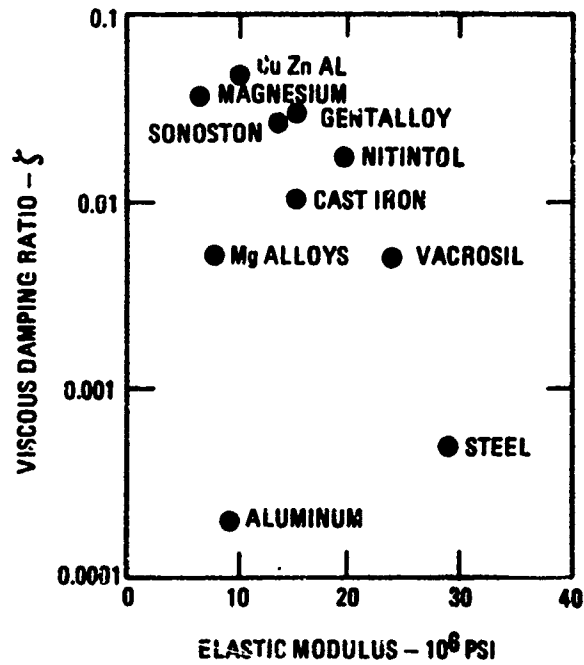


Figure 8.3. Typical damping ratio for various alloys at a stress level equal to one tenth of the yield stress as function of the elastic modulus.

TABLE 8.2 TYPICAL DAMPING VALUES IN UNIDIRECTIONAL COMPOSITES WITH AXIAL FIBERS

Material	Fiber Volume Fraction V_f	Flexural Modulus MSI	Viscous Damping Ratio ζ
Fiberglass/Epoxy	0.72	7.79	0.0005
	0.50	5.48	0.0007
Fiberglass/Polyester	0.66	6.2	0.0009
	0.54	4.95	0.0012
Kevlar/Epoxy	0.65	9.75	0.0018
HM Graphite/Polyester	0.54	25.8	0.0011
	0.61	33.6	0.0012
HT-S Graphite/LY558 Epoxy	0.60	17.9	0.00015*
	0.70	19.7	0.00012*
HT-S Graphite/F-HNA Epoxy	0.70	20.5	0.00012*
HT-S Graphite/PLA 4517 Epoxy	0.60	19	0.00053
AS1 Graphite/3501-6 Epoxy	-	-	0.0005
Celion 3000 Graphite/5208 Epoxy	-	21.1	0.00033
Celion 3000 Graphite/5213 Epoxy	-	19.7	0.00024
CY-70 Graphite/934 Epoxy	-	42.3	0.00046
HM-S Graphite/CY209 - HT972 Epoxy	0.5	22.3	0.00049
Boron/Epoxy	0.55	27.6	0.00064

*Lowest values ever measured.

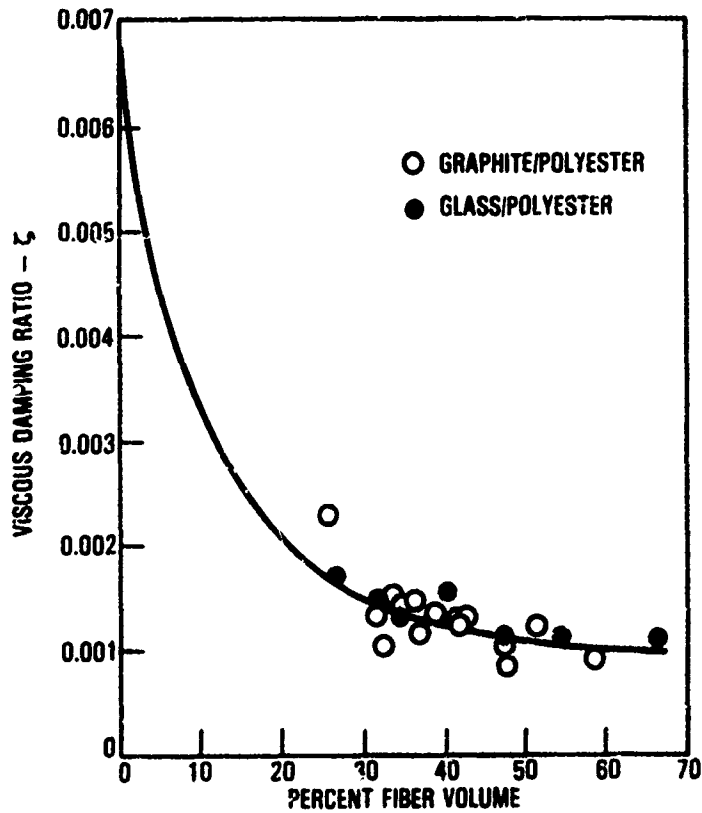
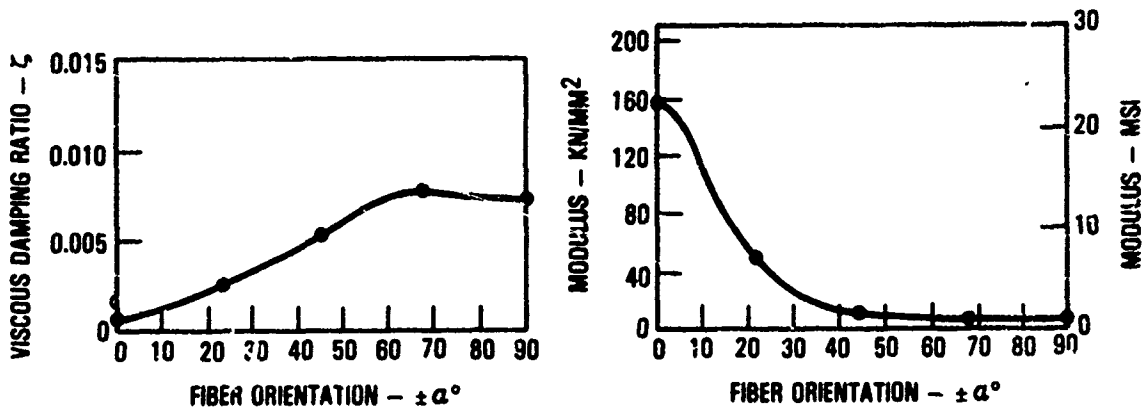


Figure 8.4. Variation of viscous damping ratio with fiber volume in early beam tests.



(b) VARIATION OF DAMPING AND YOUNG'S MODULUS WITH FIBER ORIENTATION IN THE FIRST MODE [7.75]

Figure Figure 8.5. Measured Young's modulus and damping for graphite/epoxy composite at ambient temperature.

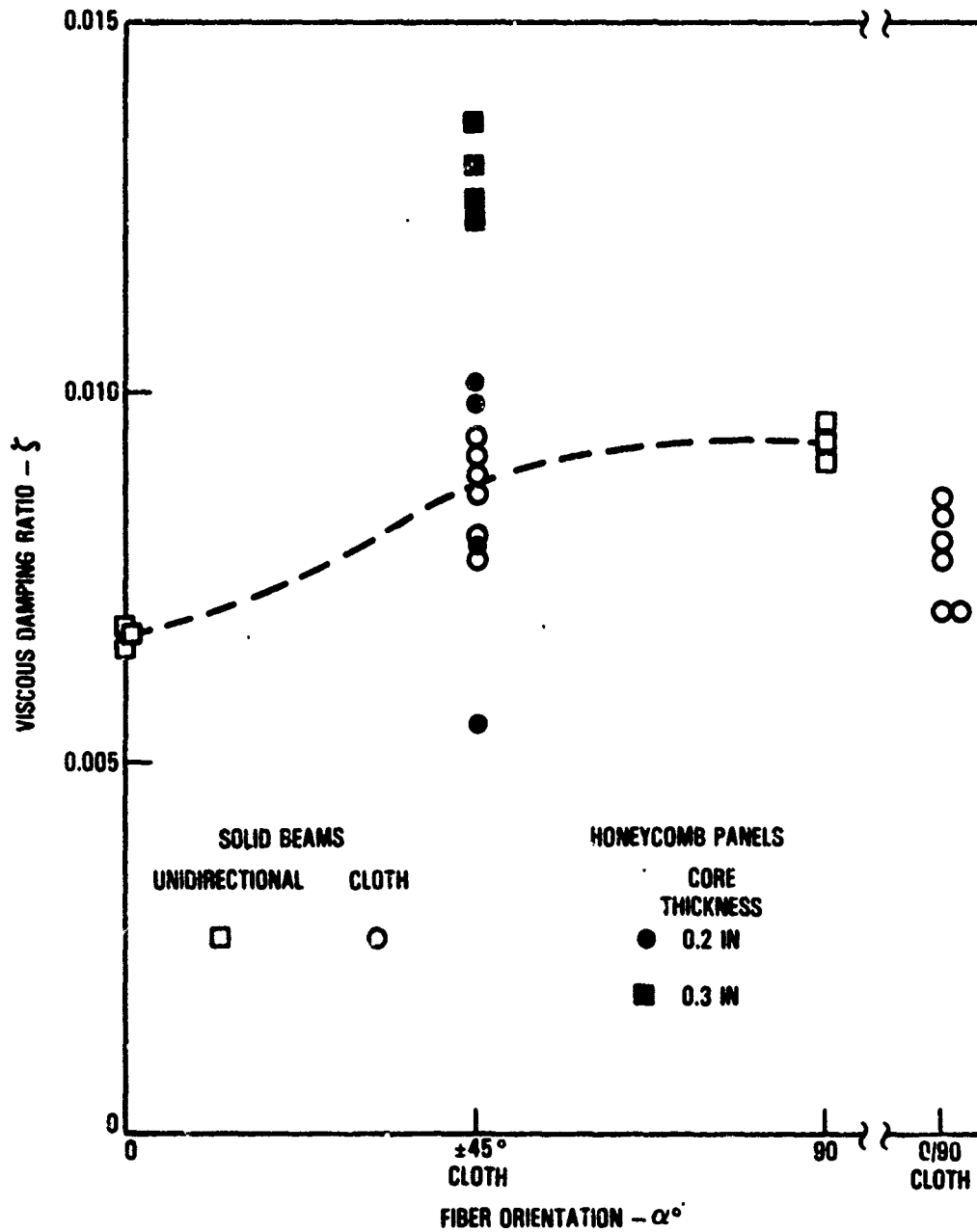


Figure 8.6. Measured damping in free-free Kevlar honeycomb panels and beams.

TABLE 8.3. EFFECT OF RESIN DAMPING ON THE DAMPING OF CHOPPED ALIGNED GRAPHITE FIBER COMPOSITE

Material Identified by Resin Number Only [8.11]	Resin		Chopped Fiber Composite ($V_f^* = 0.6$)	
	Modulus MSI	Viscous Damping Ratio, δ	Modulus	Viscous Damping Ratio, δ
1	0.144	0.075	13.25	0.004
5	0.475	0.0035	17.62	0.00025
6	0.249	0.075	16.69	0.005

*Fiber volume fraction

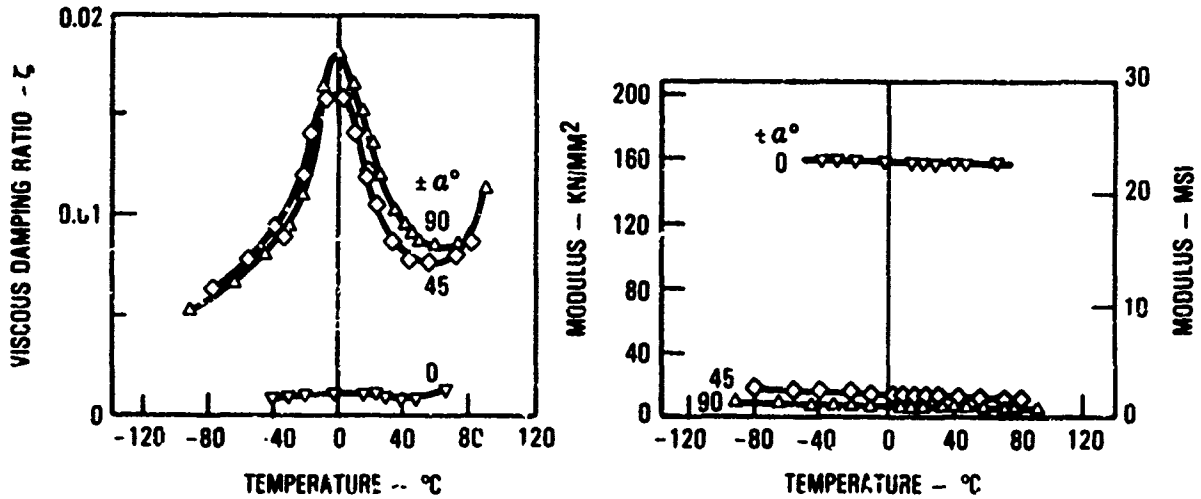


Figure 8.7. The behavior of graphite/epoxy composite, as a function of temperature.

TABLE 8.4 MATERIAL DAMPING IN METAL MATRIX COMPOSITES

Material	Fiber Volume Fraction V_f	Flexural Modulus MSI	Viscous Damping Ratio ζ
Boron BR4C/6061 Al	0.57	34.1	0.00038
P55 Graphite/6061 Al	-	26.4	0.00088
P100 Graphite/6061 Al	-	42.5	0.00085
P55 Graphite/ZE41A Mg	-	23.1	0.00070
P100 Graphite/ZE41A Mg	-	40.8	0.00065
P55 Graphite/AZ91C-Ti	-	-	0.0004
P100 Graphite/AZ91C-Ti	-	-	0.0004
P100 Graphite/AZ91C-Mg	-	-	0.0010
FP-Al ₂ O ₃ /Li Al	-	32	0.00045
FP-Al ₂ O ₃ /C.P. Mg	-	30	0.00045
FP-Al ₂ O ₃ /Ze41A Mg	-	30	0.00045
Particulate SiC/6061 Al	0.45	22	0.0002*- 0.001
Whiskers SiC/6061 Al	0.20	14.1	0.0002*- 0.001

*Damping decreases with frequency, with lower damping value at higher frequency (6000 Hz) and the higher damping value at low frequency (10 Hz).

8.2 DAMPING IN STIFFENED HONEYCOMB AND STIFFENED MULTI-BAY COMPOSITE AND METAL PANELS

8.2.1 Nature of the Damping

Stiffened multi-bay panels and stiffened honeycomb panels are typically used in secondary aircraft structures, which can also be exposed to high level acoustic loading. As a consequence, these types of structure are used in acoustic fatigue tests which represent the major source of information on the damping of these structures. A nine-bay panel, with a larger center bay, is typically used to represent the multi-bay panel. The intent is to ensure that failures occur in the periphery of the center bay and not along the test frame edges where the interpretation of the results becomes difficult. However, multi-bay panels with even stiffener spacings and even number of panels in the array have also been used. This variety of panel configurations has lead to difficulties in both identifying and interpreting the panel modes since many "fundamental" modes can exist with frequencies dependent on which adjacent panels combine in the vibration. The situation can be even more confusing for the higher modes. In contrast, stiffened honeycomb panels are tested singly on account of their large size. Modes, and damping trends of these modes, can be readily identified. Testing of stiffened honeycomb panels [8.2, 8.5] provided the conclusive experimental evidence of the near constant damping behaviour [8.1] in the fundamental mode (Figure 8.8). More recently, the trend has been towards the greater use of composites, employing fastener attached large-bay minisandwich skin construction [8.17], bonding [8.18, 8.19] or integrally stiffened construction [8.3, 8.20]. Bonding has also been used with aluminum panels [8.21, 8.22].

The highest damping is generally obtained in the fundamental mode. The damping usually falls off in level, in the higher modes of the panel, with increasing mode number. Acoustic radiation damping behaves in a similar manner. The reduction in the higher mode damping is produced by the cancellation effect. Since acoustic radiation is proportional to the area of each panel in the panel array, cancellation effect can also be obtained in a panel array in which the adjacent panels are vibrating out-of-phase with each other.

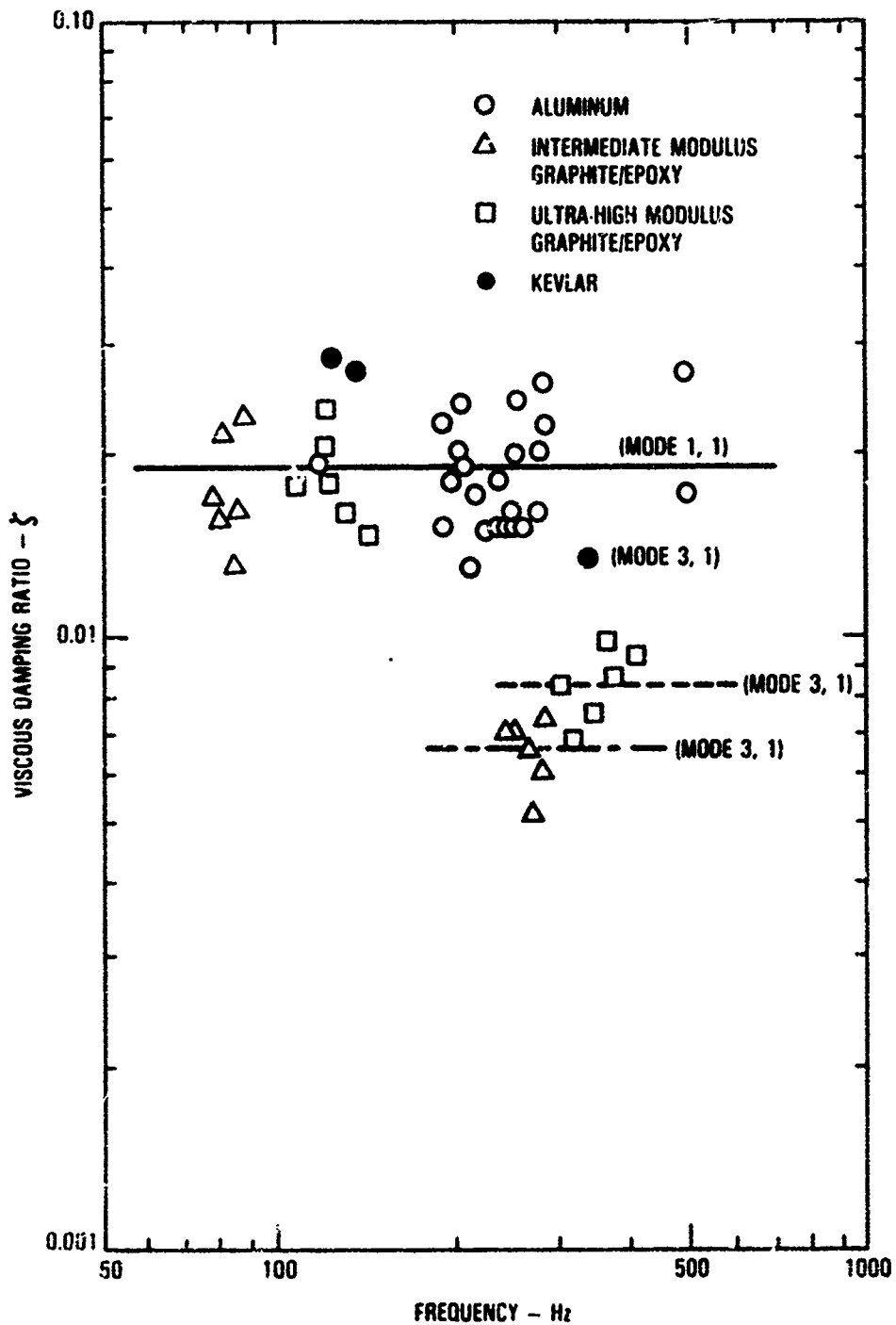


Figure P.8. Actual measured variation of fundamental mode damping with frequency for stiffened honeycomb panels.

The acoustic damping in this instance would be the acoustic damping of a single panel divided by the number of panels vibrating out-of-phase. If the panels are all vibrating in-phase then the acoustic damping is the same as that of a single panel in the array. The panels obviously have to have equal stiffener spacing for this type of response to occur.

Basically, there should be no significant difference in the damping of identical bonded metal, bonded composite or integrally stiffened metal or composite panels since the dominant source of damping is due to acoustic radiation. Kevlar composites have a significant material damping, with a viscous damping ratio of approximately 0.008 or more, which must be added to the acoustic radiation damping. Also, the friction damping at the fastener line, in fastener attached panels, must be added to the acoustic radiation damping. Even then the acoustic radiation damping still dominates. This result [8.1] is illustrated in Figure 8.9 by comparing the fundamental mode damping in multi-bay riveted panels [8.23] with that in multi-bay bonded panels [8.21]. The average damping is slightly lower for the bonded panels. The constant fundamental mode damping with frequency is also evident in the figure. The main difference is obtained in the higher panel modes where the damping at the fastener line becomes the dominant source of damping. In integrally stiffened or bonded panels, the damping level continues to drop down towards the material damping level for the layup used in the composite skin, as illustrated in Figure 8.10, or to that provided by the bonding. The material damping of a quasi-isotropic graphite/epoxy panel, with a $(0^\circ, \pm 45^\circ, 90^\circ)_s$ layup in the skin, has a viscous damping ratio around 0.0015. There is virtually no difference in the fundamental mode damping of fastener attached graphite/epoxy and aluminum panels (Figure 8.8) of similar size, although the smaller Kevlar honeycomb panels did exhibit a higher damping due to the significant contribution from the material damping. The most encouraging result is that the damping in these panels are predictable (Figures 8.10 and 8.11), subject to the usual scatter in the test data.

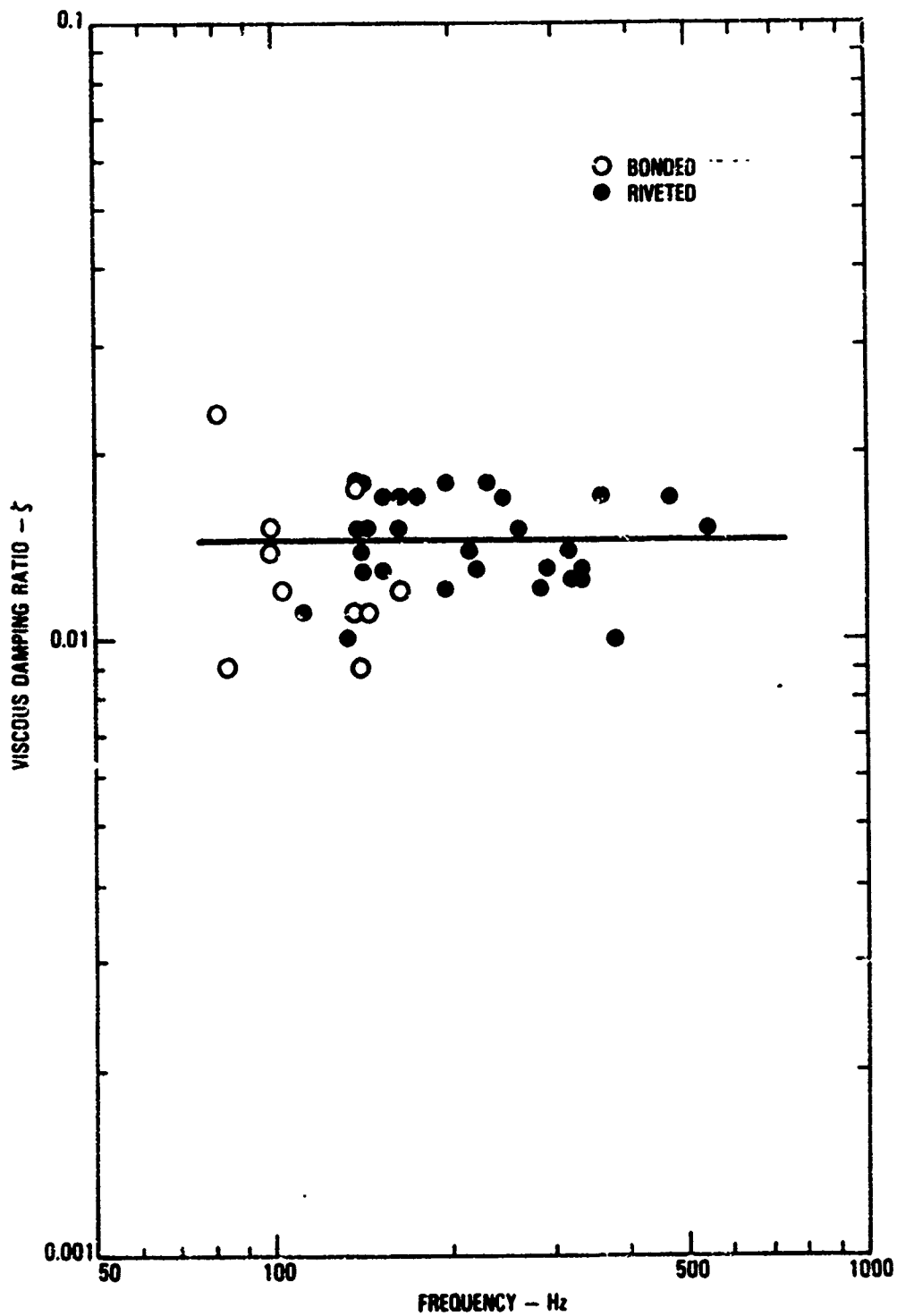


Figure 8.9. Variation of the measured damping in the fundamental mode of riveted and bonded multi-bay skin-stringer aluminum panels with frequency.

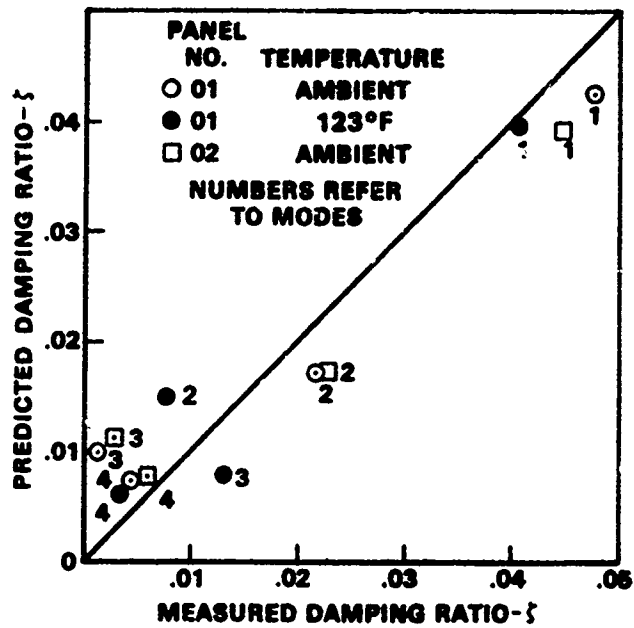


Figure 8.10. Comparison of theoretically predicted and measured viscous damping ratios of blade stiffened mini-sandwich graphite/epoxy panel.

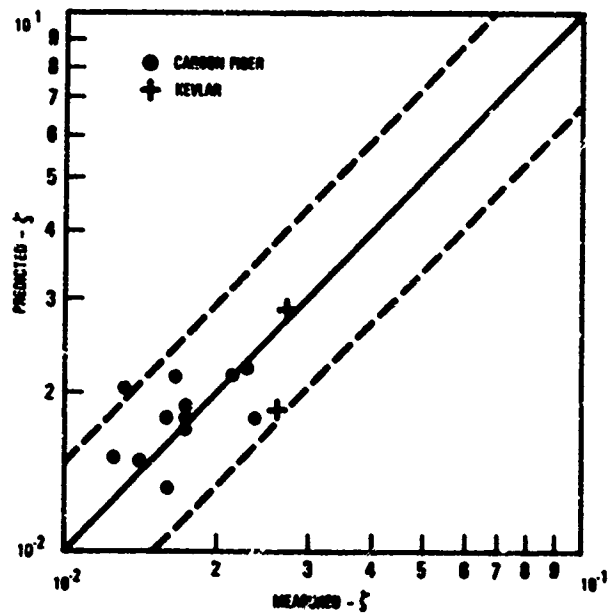


Figure 8.11. Comparison of theoretically predicted and measured viscous damping ratios for fundamental mode of stiffened composite honeycomb panels.

8.2.2 Damping Levels

The damping levels for the fundamental mode of a range of stiffened panel type structures are summarized in Table 8.5. These are the average measured damping levels. The actual damping can vary by a factor of two or more above and below this value due to scatter in the data as illustrated in Table 8.5. The damping data are least defined for multi-bay composite panels. The data that are available [8.3, 8.20, 8.21] range from a low viscous damping ratio of 0.0042 to a high value of 0.047 in the fundamental mode. Since the high damping values are generally for panels with a large center bay, these damping values are generally predictable. It is the low damping values that are least predictable. Consequently, based on the discussion in the previous section, the bonded and integrally stiffened graphite/epoxy panels are assumed to have the same average damping as the bonded aluminum skin-stringer panels. The average damping for the fundamental mode of integrally stiffened Kevlar cloth panels has been obtained by adding the average material damping from the ± 45 degree layup in Figure 8.6 to the bonded aluminum skin-stringer panel damping.

The actual measured damping for the graphite/epoxy box structure (the NASA L-1011 composite aileron) is quoted in Table 8.5. The mini-sandwich panel sizes used in the NASA L-1011 composite aileron are much larger than used in the corresponding aluminum design. Thus, a direct comparison between the damping of the aluminum box structure in Table 8.5 and that from the composite aileron is probably not valid.

Chemical milling has the effect of increasing the resonant frequency of the panel relative to a panel with the unmilled skin. Since the fundamental mode damping of a stiffened panel is, basically, unaffected by frequency, the damping in the chemically milled panel is assumed (Table 8.5) to be the same as that of a conventional skin-stringer panel.

8.2.3 Method for Predicting the Damping of Skin-Stringer Type Panels

The method for predicting the damping of the skin-stringer panels is the same as that described in Reference [8.1]. For simplicity, the panel array

TABLE 8.5 FUNDAMENTAL MODE VISCOUS DAMPING RATIO FOR METAL AND COMPOSITE STIFFENED PANEL TYPE STRUCTURES

Structures	Average Viscous Damping Ratio ζ	Typical Range of Measured Data	
		Minimum ζ	Maximum ζ
Riveted aluminum skin-stringer panels both flat and curved with and without seaiaant	0.0145	0.005	0.05
Riveted titanium skin-stringer panels	0.0145	0.008	0.03
Riveted aluminum box structure	0.0145	0.008	0.04
Bonded aluminum skin-stringer panels	0.0125	0.009	0.022
Bonded and integrally stiffened graphite/epoxy panels	0.0125	0.0042	0.047
Bonded and integrally stiffened Kevlar cloth panels	0.020*	0.012*	-
Graphite/epoxy box structure assembled with fasteners	0.004	Only one tested	
Fastener attached stiffened metal and graphite/epoxy honeycomb panels	0.019	0.013	0.027
Fastener attached stiffened Kevlar honeycomb panels	0.027	Only two tested	
Corrugated and closely spaced hat stiffened aluminum panel structure	0.017	0.014	0.019
Built-up aluminum structures with integrally machined skins	0.0057	0.0019	0.0145
Riveted chemically milled aluminum panels (expected to be the same as skin-stringer panels but at higher frequency).	0.0145*	-	-

*Estimated.

is assumed to have a large center bay which produces the dominant vibration response and, therefore, the highest rms strain level to excitation such as random acoustic loading. In the most general panel, the damping is composed of three parts. These are the acoustic radiation damping, the fastener-like friction damping and the material damping represented by the viscous damping ratios ζ_a , ζ_F and ζ_M , respectively. The viscous damping ratio, ζ_{mn} , in the m, n^{th} mode of a skin-stringer type panel is given by

$$\zeta_{mn} = \zeta_a + \zeta_F + \zeta_M \quad (8.1)$$

The material damping is obtained from previously described beam tests for the particular layup used in the composite panel. It is usually taken as zero for graphite/epoxy and aluminum panels. The material damping for a Kevlar panel with a $\pm 45^\circ$ cloth layup is given approximately by $\zeta_M = 0.008$.

The viscous damping ratio due to acoustic radiation can be calculated from the equation

$$\zeta_a = \frac{64}{\pi} \frac{\rho}{4} \frac{f_n}{c} \frac{1}{M} \frac{a}{m} \frac{b}{n} \quad (8.2)$$

where

- ρ = density of air
- c = speed of sound in air
- f_n = natural frequency of the m, n^{th} mode
- M = panel surface density
- a, b = panel length and width
- m, n = mode number in the length and width direction respectively

The viscous damping ratio due to friction at the fastener line is given approximately by [8.1]

$$\zeta_F = 0.0253 \frac{s(a+b) - \frac{n}{s} - \frac{m}{s}}{ab} \quad (8.3)$$

where s is the number of fasteners per inch and the other dimensions are

also given in inches. The above equation is based on a viscous damping ratio of 0.0085 measured on a particular panel array under near vacuum conditions. A viscous damping ratio of only 0.0034 has been measured on a large unbaffled curved panel array. The friction damping is considered to produce the greatest scatter in the data due to variability in the fabrication of the panels. Consequently, the constant term in equation 8.3 can be adjusted to reflect actual measured friction damping levels. For bonded aluminum and composite panels, and integrally stiffened composite panels, $\zeta_F = 0$. The degree of correlation achieved by this method is illustrated in Figure 8.12 and in Figure 8.13 for the fundamental mode of two typical panels.

The damping in the higher order modes of a panel can be predicted using the average fundamental mode viscous damping ratio in Table 8.5 for the appropriate stiffened structure, the fundamental mode resonant frequency of the panel and the resonant frequency of the higher mode. The viscous damping ratio for the m,n^{th} mode is given by

$$\zeta_{mn} = (\zeta_{11} - \zeta_M - \zeta_F) \left(\frac{f_{mn}}{f_{11}} \cdot \frac{1}{m^2 n^2} \right) + \zeta_M + \zeta_F \quad (8.4)$$

where

- ζ_{mn} = m,n^{th} mode viscous damping ratio
- ζ_{11} = fundamental mode viscous damping ratio
- ζ_M = contribution from material damping
- ζ_F = contribution from friction damping of the rivet line (equation 8.3)
- f_{mn} = m,n^{th} mode resonant frequency
- f_{11} = fundamental mode resonant frequency

Typical higher mode viscous damping ratios predicted by equation 8.4 are illustrated in Figure 8.13.

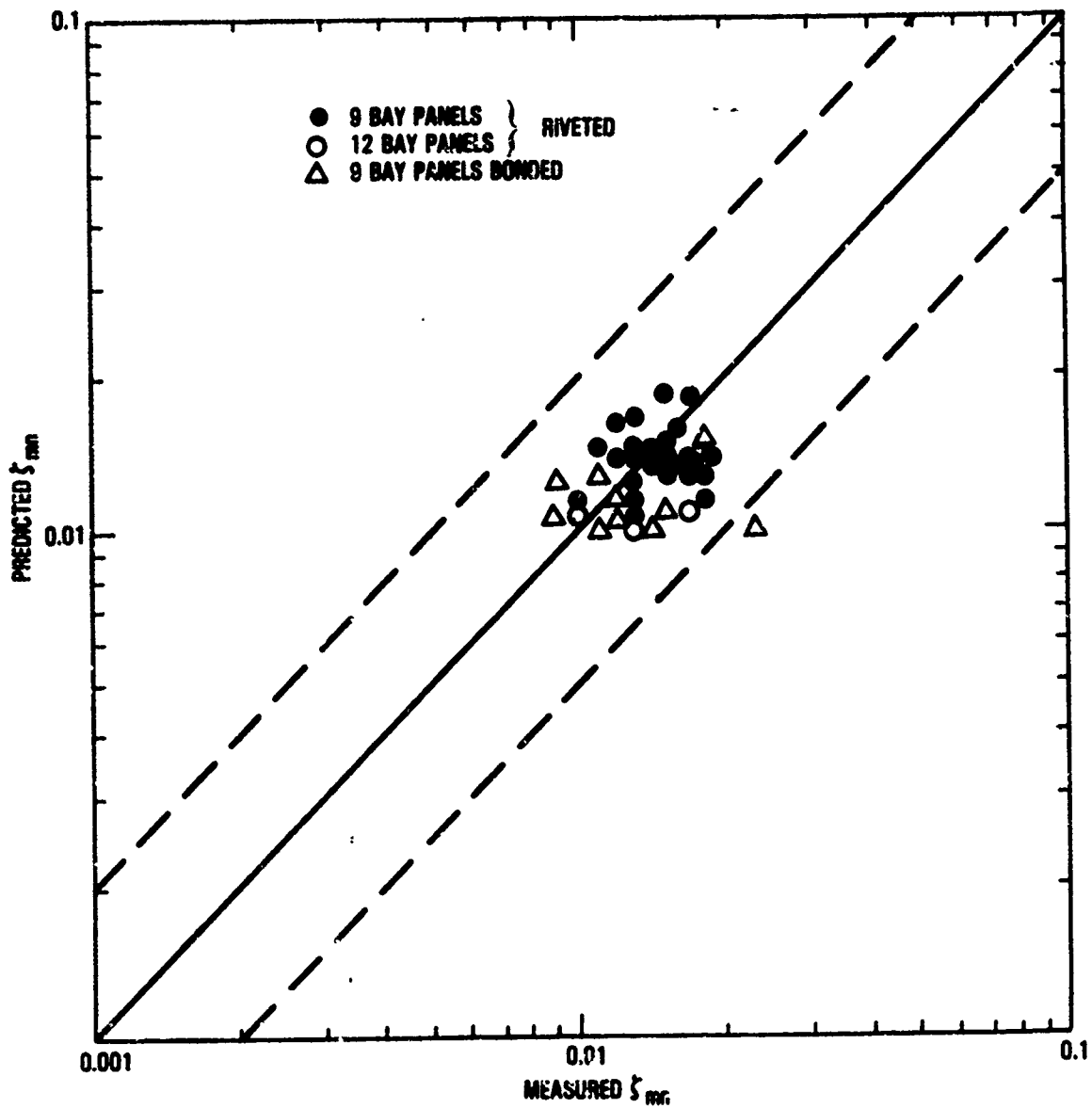


Figure 8.12. Comparison of measured and predicted damping in the fundamental mode of riveted and bonded multi-bay skin-stringer aluminum panels.

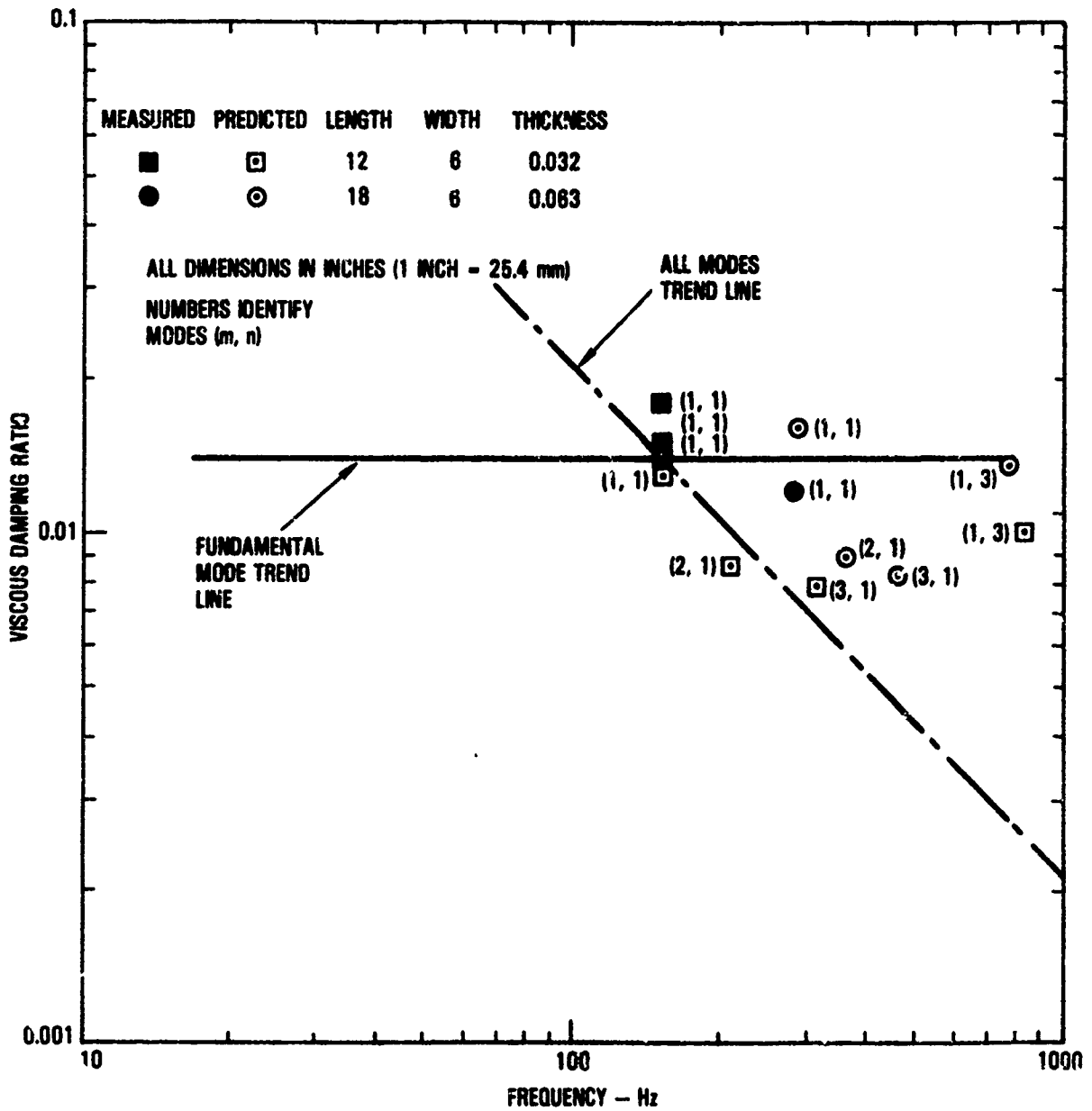


Figure 8.13. Comparison of measured and predicted damping of riveted multi-bay aluminum panels with predictions for higher mode damping.

8.2.4 Effect of Axial and Shear In-Plane Loads on Stiffened Panels Damping

The damping of stiffened panels under axial in-plane loading [8.24] remains constant with axial tension load, but increases with compression on approaching buckling. The damping of the panel becomes nonlinear on approaching buckling as indicated by a change in the rate of the free decay response with amplitude. The damping of the stiffened panel also increases with in-plane shear load on approaching panel buckling [8.25], as illustrated in Figure 8.14 for an integrally J-stiffened mini-sandwich panel. The damping in noncritical modes also increases on approaching shear buckling. Typical variation of the modal frequencies with shear load is illustrated in Figure 8.15.

8.2.5 Effect of Fluid Loading on Stiffened Panel Damping

The effect of fluid loading on the damping of stiffened steel panels [8.26] with welded T-section stiffeners is illustrated in Figure 8.16. There is virtually no difference in the damping of the panel when in air or when in contact, on one side, with water. There is a shift in frequency due to a combination of mass loading and hydrodynamic pressure. The one-over-the-frequency type trend line is due to the presence of higher order modes.

8.3 DAMPING IN STIFFENED SHELLS

The viscous damping ratios measured on two untrimmed aircraft fuselage shells [8.27, 8.28] and on a small diameter stiffened cylinder [8.29], both with and without acoustic trim, are illustrated in Figure 8.17. The damping data for all three of the untrimmed shells appear to collapse onto a single curve. The interior acoustic trim, even when not in contact with the shell skin, does appear to increase the damping approximately by a factor of four over the bare shell damping. The one-over-the-frequency trend line is again due to the presence of higher order modes.

8.4 DAMPING IN SPACECRAFT AND ROCKETS

Typical damping data measured during ground vibration tests on unmanned spacecraft [8.30, 8.31] are illustrated in Figures 8.18 and 8.19. The limited damping data [8.30] measured on a spinning satellite indicate that

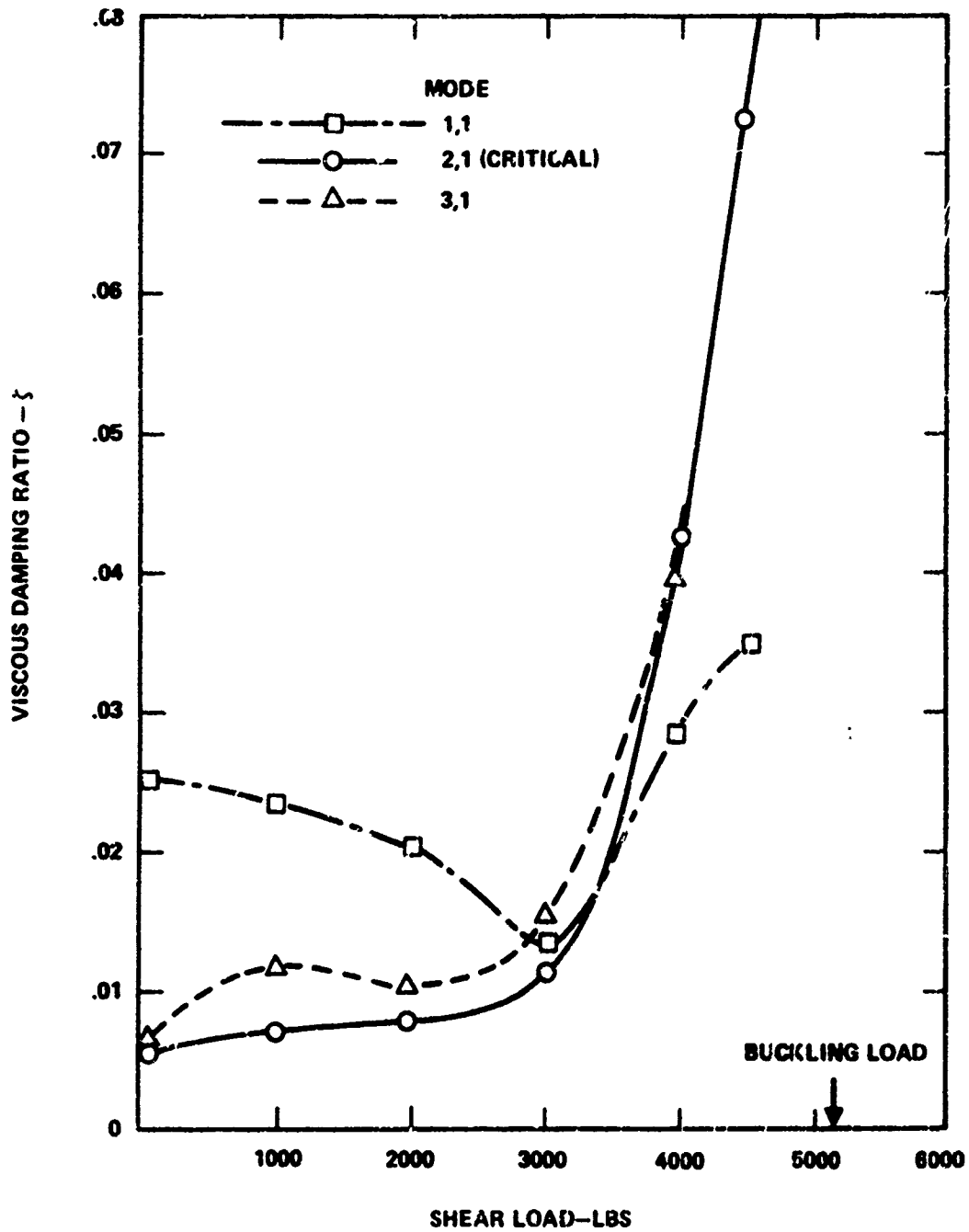


Figure 8.14. Variation of damping with Jack load for J-stiffened mini-sandwich panel.

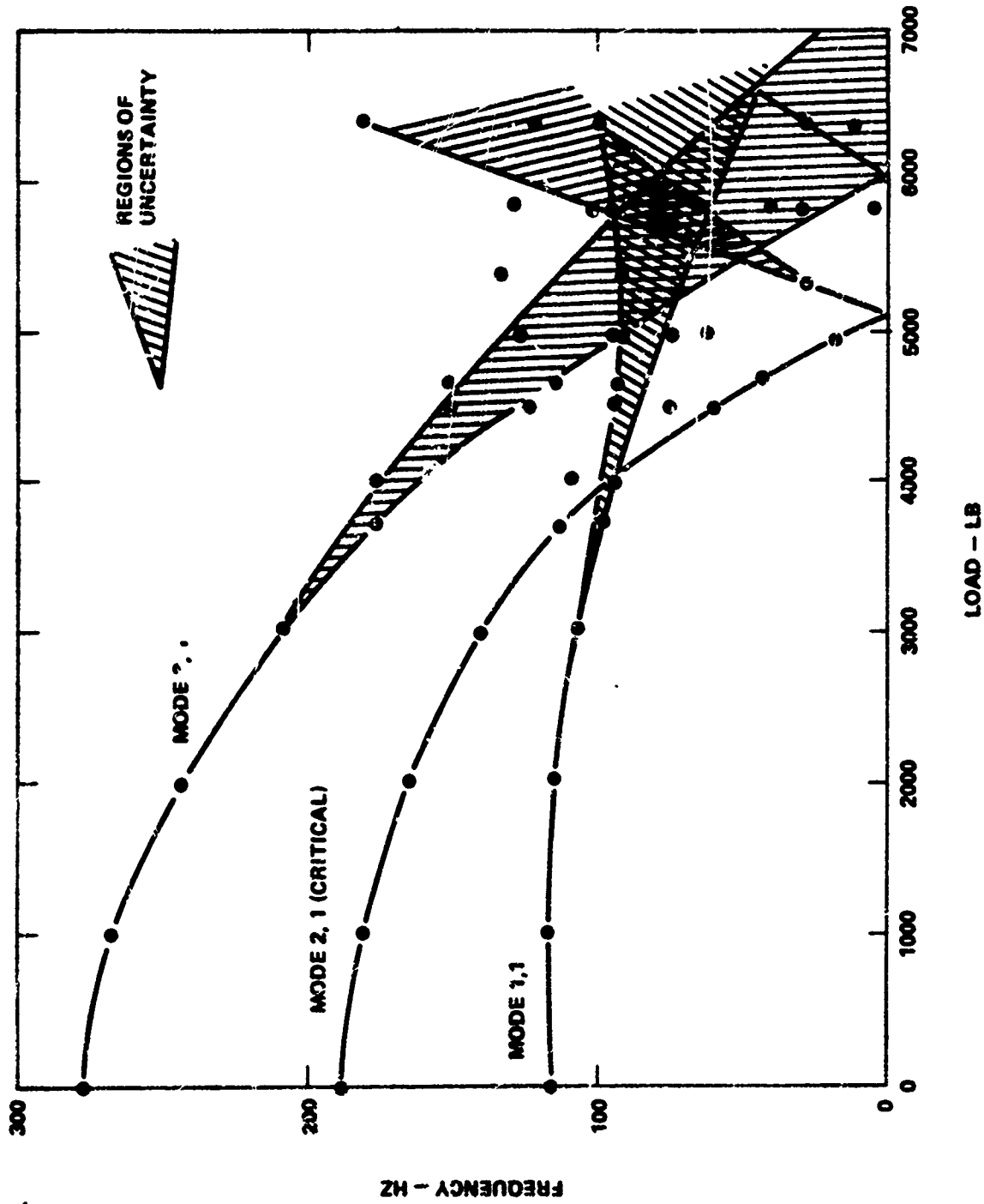


Figure 8.15. Variation of the J-stiffened mini-sandwich panel resonant frequencies with Jack load.

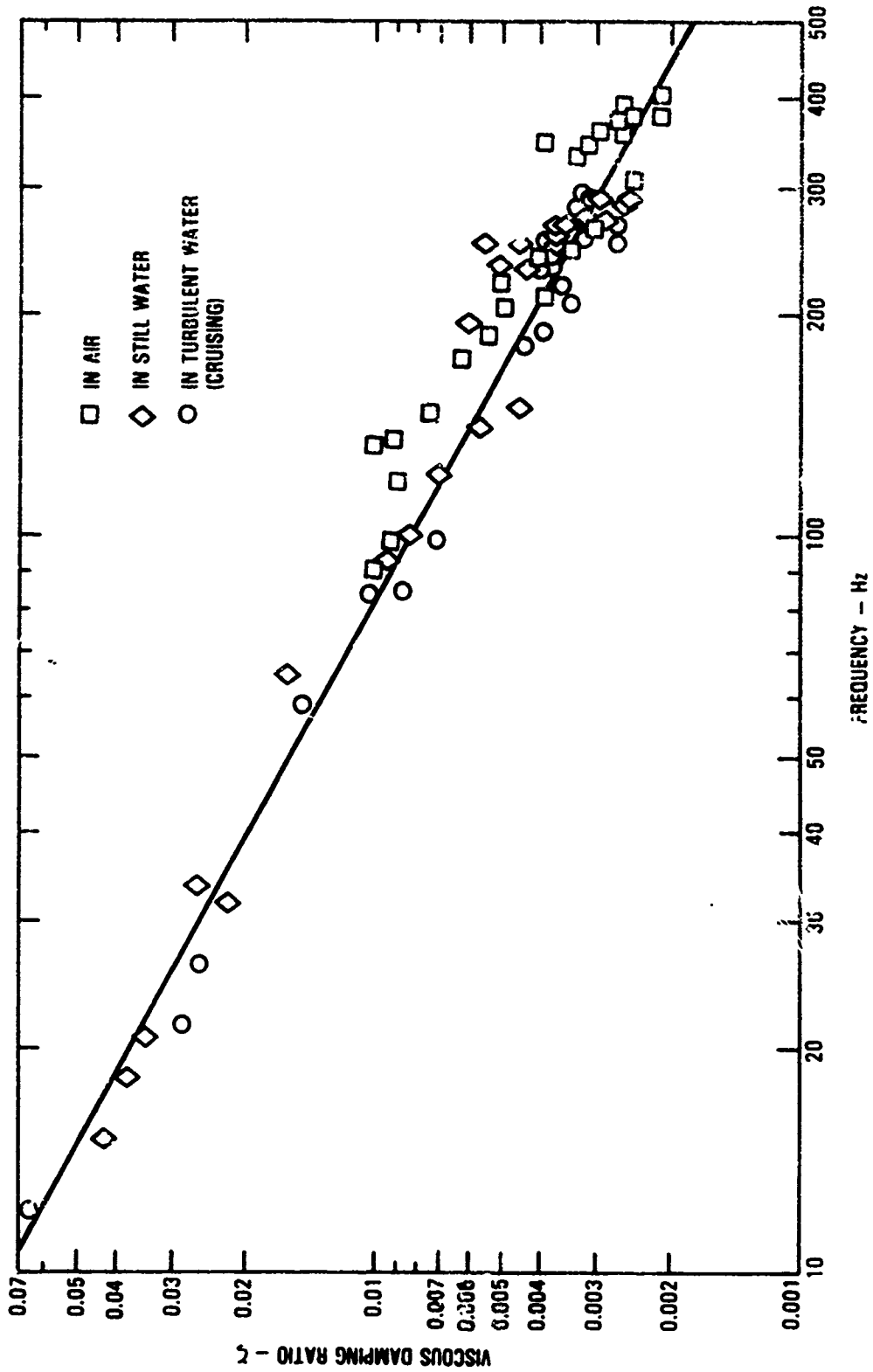


Figure 8.16. Damping measured on a welded stiffened steel structure in air and immersed in water.

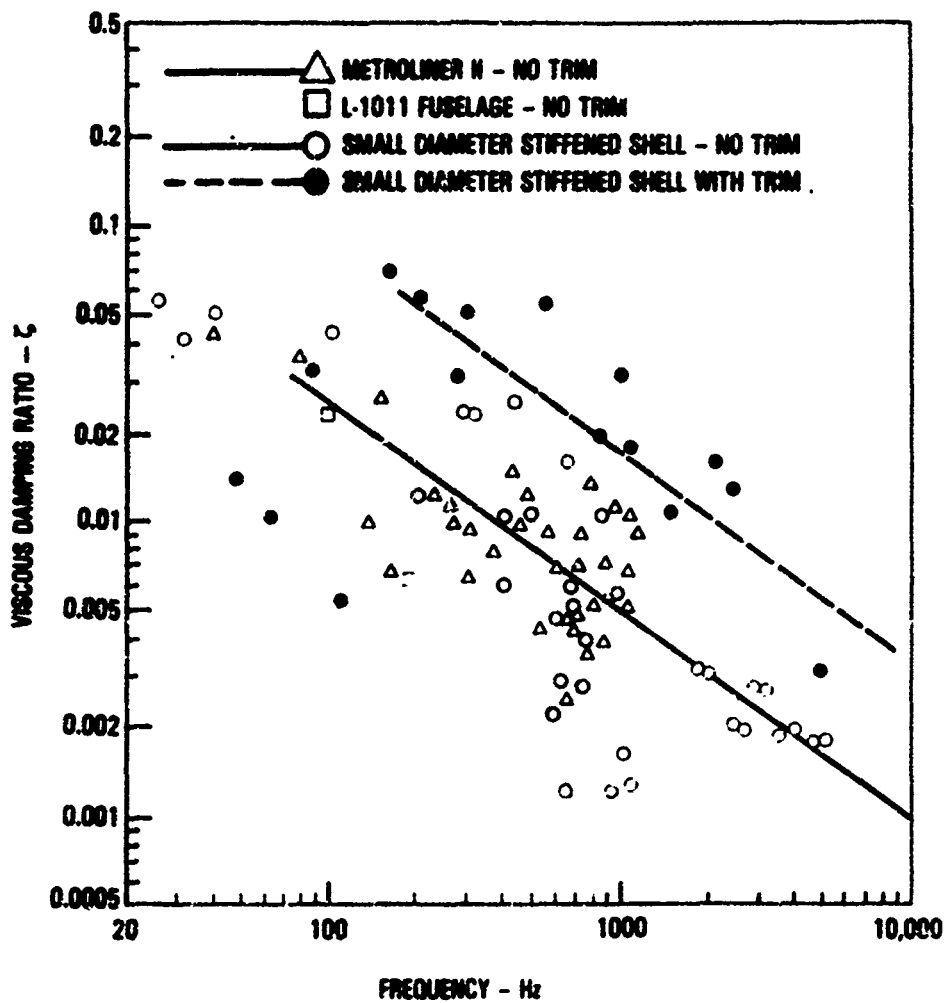


Figure 8.17. Damping measured on bare stiffened shells and a trimmed stiffened shell as a function of frequency.

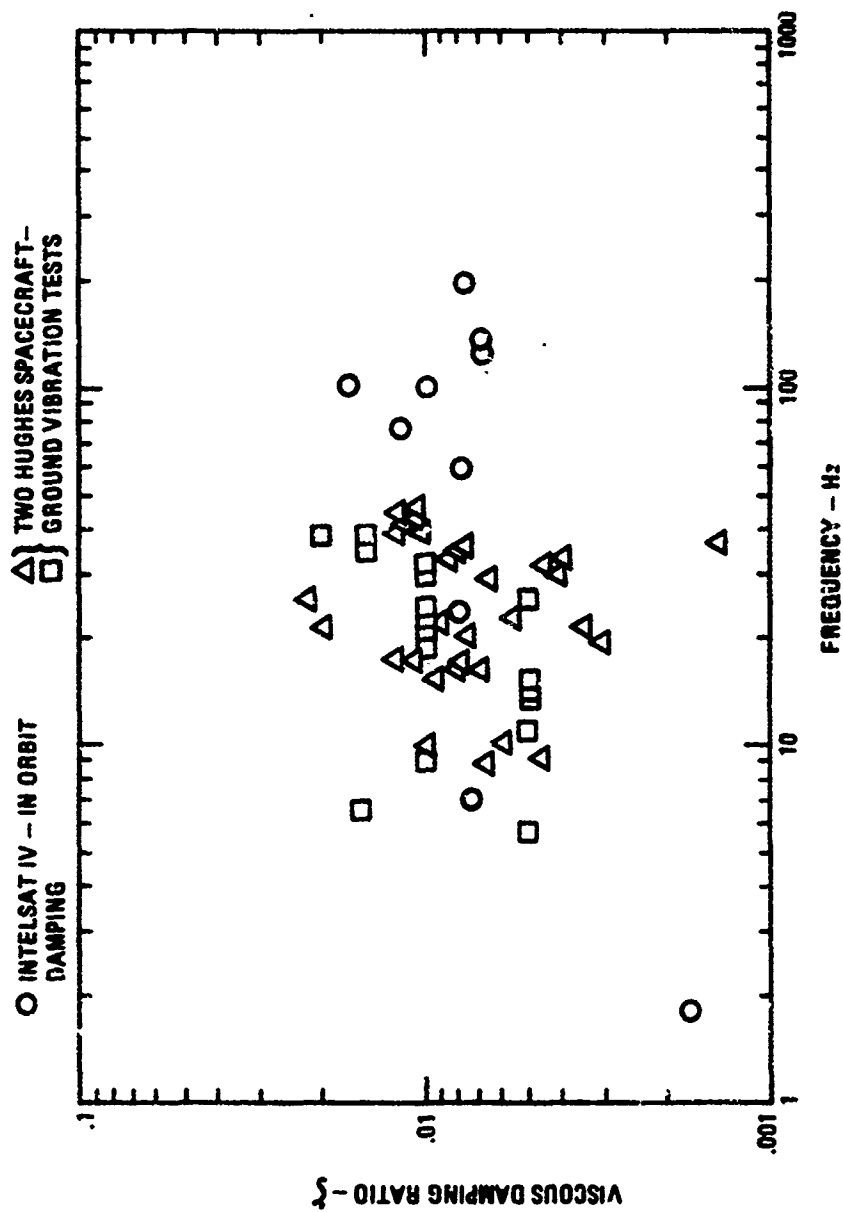


Figure 8.18. Comparison of typical damping levels measured on the ground and in orbit.

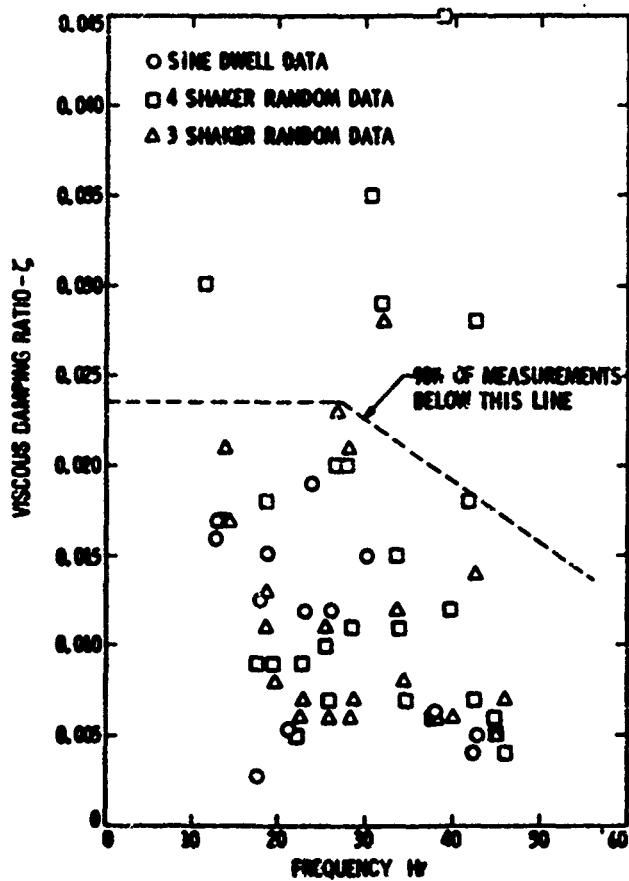


Figure 8.19. Typical damping levels measured during Galileo spacecraft modal tests.

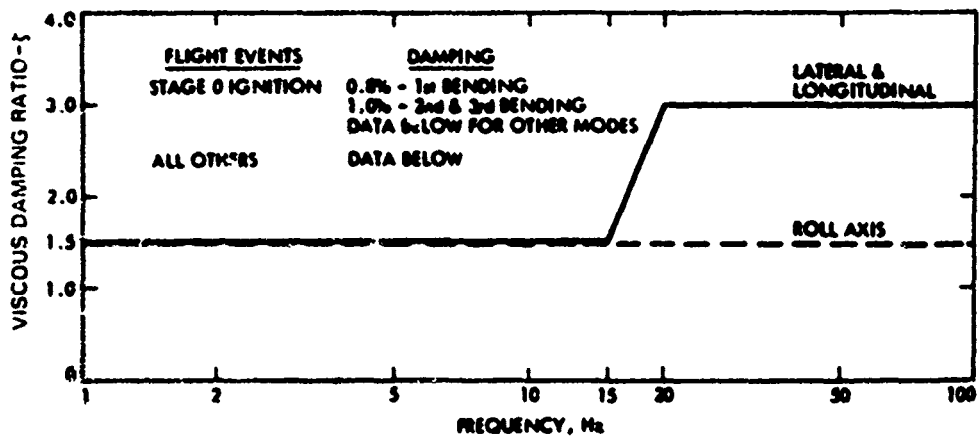


Figure 8.20. Damping schedule for Titan launch vehicle.

similar damping levels (Figure 8.18) are also obtained in orbit. Friction damping in the joints is the main source of damping in these spacecraft, both on the ground and in orbit.

Typical damping schedule [8.30] of a rocket, used to launch some of the unmanned spacecraft, is illustrated in Figure 8.20. Damping levels measured on the space shuttle ascent vehicle [8.32] currently used to launch unmanned spacecraft, are illustrated in Figure 8.21.

8.5 DAMPING IN JET ENGINE COMPONENTS

Typical damping levels in jet engine components taken from Section 6 of this volume are summarized in Table 8.6.

8.6 DAMPING IN PRINTED CIRCUIT BOARDS

Typical measured damping in printed circuit boards [8.33, 8.34] is summarized in Table 8.7. A method for predicting the circuit board damping [8.33] is also contained in the table.

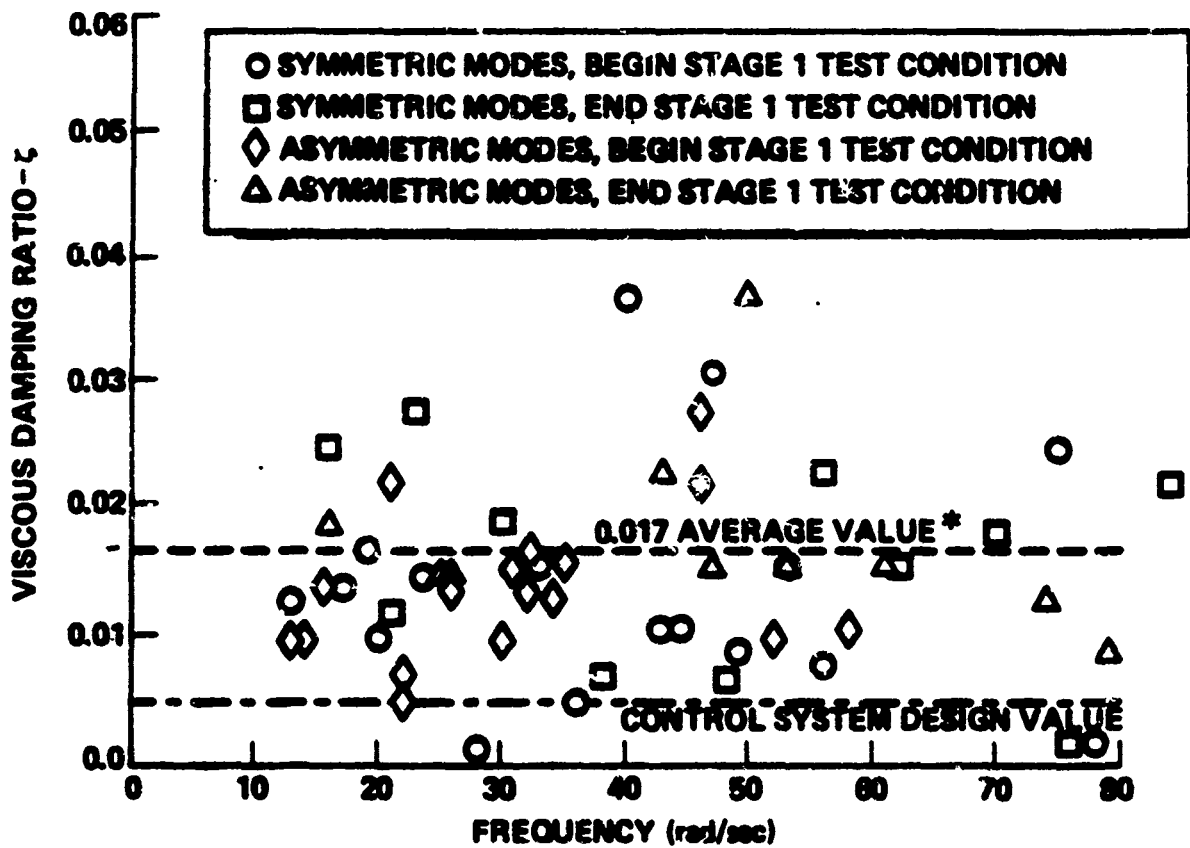


Figure 8.21. Equivalent viscous damping ratios measured during space shuttle ascent vehicle Stage 1 vibration test.

TABLE 8.6. MEASURED DAMPING VALUES FOR ENGINE COMPONENTS

Description of Structure	Frequency Hz	Viscous Damping Ratio - ζ
TF-41 Jet Engine Inlet Extension	3140	0.0011 to 0.0027*
RF-33-P3 Turbojet Engine Welded Inlet Guide Vanes (IGV) and Shrouds	1000 to 5000	0.0012 to 0.0023*
Engine Rear Mount Ring	374 403 903 1172 1396 3515 4325	0.0037 0.0033 0.0045 0.0030 0.0037 0.0040 0.0049
TF-30 Jet Engine Welded Titanium Guide Vanes	3000 to 4000	0.0009 to 0.0018*
Helicopter Turbine Engine Exhaust Stacks	50 to 500	0.0005 to 0.005
Jet Engine Turbine Blade	746 Bending } 824 Torsion }	0.001 to 0.002
Exducer - Turbing Blade Assembly	5300 8500	0.0022 to 0.0039* 0.0009 to 0.0014

*Damping varies with temperature

TABLE 8.7. TYPICAL RANGE OF MEASURED PRINTED CIRCUIT BOARD DAMPING VALUES

Frequency f_n Hz	ζ	Q	K	Reference
65	0.0142	35	4.3	8.34
165	0.023	22	1.71	8.34
215 (2g's input)	0.033	15	1.023	8.33
182 (5g's input)	0.045	11.2	-	
161 (10g's input)	0.061	8.2	-	
<p>Empirical relationship [8.33]</p> $Q \approx K (f_n)^{1/2}$ $\zeta = \frac{1}{2Q}$ <p style="text-align: right;">K \approx 0.5 \rightarrow 2 Typical Input 2g's and less</p>				

REFERENCES

- 8.1 Soovere, J., "Method for Predicting the Damping in Stiffened Structures", Paper to be Presented at the Vibration Damping Workshop II, Las Vegas, 5-9 March 1986.
- 8.2 Soovere, J., "Dynamic Properties of Graphite Fibre Honeycomb Panels", AIAA Dynamics Specialists Conference, Williamsburg, Virginia, March 1973, Paper No. 73-326.
- 8.3 Soovere, J., "Effect of Acoustic/Thermal Environments on Advanced Composite Fuselage Panels", Journal of Aircraft, Volume 22, No. 4, April 1985.
- 8.4 Soovere, J., "Dynamic Response and Acoustic Fatigue of Stiffened Composite Structures", Proceeding of the Second International Conference on Recent Advances in Structural Dynamics, M. Petyt and H.F. Wolfe Editors, University of Southampton, 9-13 April, 1984, p. 775.
- 8.5 Soovere, J., "Dynamic Response of Acoustically Excited Stiffened Composite Honeycomb Panels", Ph.D. Thesis, Institute of Sound and Vibration Research, Southampton University, England, March 1984.
- 8.6 Lazan, B.J., "Damping of Materials and Members in Structural Mechanics", Oxford: Pergamon Press, 1968.
- 8.7 Birchak, J.R., "Damping Capacity of Structural Materials", Published After 1976 - Babcock and Wilcox, Lynchburg Research Center.
- 8.8 Vandeurzen, U., "Identification of Damping in Materials and Structures - Optimization of the Dynamic Behavior of Mechanical Structures", A University of Leuven Report, Leuven, Belgium.

- 8.9 Adams, R.D., Fox, M.A.O., Flood, R.J.L., Friend, R.J. and Hewitt, R.L., "The Dynamic Properties of Unidirectional Carbon and Glass Fiber Reinforced Plastics in Torsion and Flexure", J. Composite Materials, Vol. 3, October 1969, p. 594.
- 8.10 Georgi, H., "Dynamic Damping Investigations on Composites", Damping Effects in Aerospace Structures, AGARD-CP-277, October 1979.
- 8.11 White, R.G. and Palmer, T.A., "Control of the Material Properties and Structural Application of Carbon Fiber-Reinforced Plastics", 24th Structures, Structural Dynamics and Materials Conference, Lake Tahoe, Nevada, May 2-4, 1983, Paper No. 83-859.
- 8.12 White, R.G., "Some Measurements of the Dynamic Properties of Mixed Carbon Fiber Reinforced, Plastic Beams and Plates", Aeronautical Journal, July 1975, p. 318.
- 8.13 Gibson, R.F., Suarez, S.A. and Deobald, L.R., "Improvement of Damping in Fiber-Reinforced Polymer Composites", Vibration Damping 1984 Workshop Proceedings, Dr. Lynn Rogers Editor, AFWAL-TR-84-3064, November 1984, p. S-1.
- 8.14 Ni, R.C. and Adams, R.D., "The Damping and Dynamic Moduli of Symmetric Laminated Composite Beams - Theoretical and Experimented Results", J. Composite Materials, Vol. 18, March 1984.
- 8.15 Bert, C.W. and Sin, C.C., "Sinusoidal Response of Composite - Material Plates with Material Damping", Journal of Engineering for Industry, May 1974, p 603.

- 8.16 Timmerman, N.S. and Doherty, J., "Loss Factors Measured in Metal Matrix Composite Materials", AMMRC-TR-84-22, June 1984.
- 8.17 Soovere, J. "Sonic Fatigue Testing of the NASAL-1011 Composite Aileron", The Shock and Vibration Bulletin, No. 50, Part 4, September 1980.
- 8.18 Holehouse, Ian, "Sonic Fatigue Design Techniques for Advanced Composite Aircraft Structures", AFWAL-TR-80-3019, April 1980.
- 8.19 Jacobson, M.J., "Advanced Composite Joints: Design and Acoustic Fatigue Characteristics" AFFDL-TR-71-127.
- 8.20 Jacobson, M.J.. "Fatigue of V/STOL Composite Fuselage Panels Under Acoustic-Thermal Environments", NADC-81045-60, March 1981.
- 8.21 Jacobson, M.J., "Sonic Fatigue Design Data for Bonded Aluminum Aircraft Structures", AFFDL-TR-77-45, June 1977.
- 8.22 Wolfe, H.F. and Holehouse, I., "Durability of Adhesively Bonded Structures Subjected to Acoustic Loads", AGARD Report No. 701, December 1981.
- 8.23 Ballentine, J.R., Rudder, F.F., Mathis, J.T. and Plumblee, H.E., "Refinement of Sonic Fatigue Structural Design Criteria", AFFDL-TR-67-156, January 1968.
- 8.24 Soovere, J. and Chiu, S.T., "Effect of Combined Acoustics and Flight Loads on Crack Growth", AFFDL-TR-76-68, July 1976.
- 8.25 Soovere, J., "Dynamic Response of Flat Integrally Stiffened Graphite/Epoxy Panels Under Combined Acoustic and Shear Loads", Recent Advances in Composites in the United States and Japan, J.R. Vinson and M. Taya Editors, ASTM Special Technical Publication 864, July 1985.

- 8.26 White, R.G., "The Application of a Transient Test Technique to the Study of the Local Vibration Characteristics of Ship Structures", I.S.V.R. Technical Report No. 31, May 1970.
- 8.27 Prydz, R.A., Revelle, J.D., Hayward, J.L. and Balena, F.J., "Evaluation of Advanced Fuselage Design Concepts for Interior Noise Control on High Speed Propeller-Driven Aircraft", NASA Contractor Report 165960, September 1982.
- 8.28 Socvere, J., "High Modulus Graphite Fiber Constrained Layer Damping Treatment for Heavy Aerospace Structure", AFFDL-TM-78-78-FBA, July 1978.
- 8.29 Pope, L.D. and Wilby, E.G., "Analytical Prediction of the Interior Noise for Cylindrical Models of Aircraft Fuselages for Prescribed Exterior Noise Fields (Part II), NASA Contractor Report 165869, April 1982.
- 8.30 Wada, B.K., "Spacecraft Damping Considerations in Structural Design", AGARD-CP-277, October 1979, pp. 6-1.
- 8.31 Chen, J.C., "Evaluation of Modal Test Methods", AIAA Dynamics Specialists Conference, Palm Springs, California, May 1984, Paper No. 84-1071.
- 8.32 Jensen, D.L., "Structural Damping of the Space Shuttle Orbiter and Ascent Vehicles", Vibration Damping 1984 Workshop Proceedings, Dr. Lynn Rogers Editor, AFWAL-TR-84-3064, p. Z-2.
- 8.33 Steinberg, D.S., "Vibration Analysis for Electronic Equipment", John Wiley and Sons, 1973.
- 8.34 Medaglia, J.M., "Dynamic Integrity Methods Including Damping for Electronic Packages in Random Vibration", General Electric Space Division.